PNAS
www.pnas.org

Supplementary Information for

Virion structure and genome delivery mechanism of sacbrood honeybee virus

Michaela Procházková, Tibor Füzik, KarelŠkubník, Jana Moravcová, Zorica Ubiparip, Antonín P řidal, Pavel Plevka

Pavel Plevka
E-mail: pavel.plevka@ceitec.muni.cz

This PDF file includes:

www.pnas.org/cgi/doi/10.1073/pnas.1722018115

Supporting Information Text

Supplementary methods

Virus propagation. Color and the structural features of the cell caps were used to identify the brood areas with white-eyed pupae, which were carefully extracted from the brood combs to prevent injury. The pupae were placed on paper furrows with their ventral side up. SBV (from north Moravian locality Petrusov - 49.8148567N and 16.7352783E, Czech Republic) inoculum (1 μl) was injected into pupae using a Hamilton glass micropipette with a 30-gauge, 22 mm-long needle through the inter-segmental cuticle between the 4^{th} and 5^{th} sternite. The optimal concentration of the virus in the inoculum was determined empirically by comparing virus yields when using different virus concentrations in the inoculum. Inoculated pupae were placed into Petri dishes and incubated at 30°C and 75% relative humidity for 5 days. The high-titer SBV infection resulted in a discoloration of the central part of the eyes (Fig. S11). After incubation, the pupae were frozen at -20°C. For long-term storage, the pupae were kept at -80°C.

Virus purification. Thirty experimentally infected honeybee pupae were homogenized with a Dounce homogenizer (piston–wall distance 0.075 mm) in 30 ml of phosphate-buffered saline (PBS), pH 7.4 (Sigma-Aldrich). The extract was centrifuged at 15,000 g for 30 min at 10°C. The pellet was discarded and the supernatant ultracentrifuged at 150,000 g for 3 h in a Ti50.2 fixed-angle rotor (Beckman-Coulter™). The resulting pellet was re-suspended in PBS to a final volume of 5 ml. $MgCl_2$ was added to a final concentration of 5 mM as well as 20 μg/ml DNAse I, and 20 μg/ml RNAse. The solution was incubated for 30 min at room temperature and centrifuged at 5,500 g for 15 min. The resulting supernatant was separated on a CsCl (0.6 g/ml) gradient in PBS by ultracentrifugation for 16 h at 30,000 RPM in an SW40 rotor. Opalescent bands corresponding to the virus were collected by piercing the ultracentrifuge tubes with an 18-gauge needle. The viruses were buffer-exchanged to PBS and concentrated using centrifugal filter units. This procedure yielded about 80 μg of virus with purity sufficient for crystallization and cryo-EM data collection.

Crystallization of SBV virion. SBV crystallization screening was performed at 20°C using the virus in PBS at a concentration of 6 mg/ml. Crystallization conditions were tested with the sitting-drop vapor diffusion method in 96-well plates. Cubic crystals with a size of approximately 0.08 mm were obtained by the hanging drop method in 24-well plates by mixing 1.5 μl of virus suspension with 1.5 μl of bottom solution containing 0.05 M magnesium chloride, 0.1 M MES, 8% (v/v) isopropanol, and 4% (w/v) PEG 4,000.

SBV diffraction data collection, structure determination and refinement. For data collection, SBV virion crystals were soaked in mother liquor containing 20% MPD for 1 min and immediately vitrified in liquid nitrogen. Data were collected from a single crystal at 100 K using the Pilatus 6M (Dectris) detector on beamline Proxima 1 at the Soleil synchrotron radiation source in Paris, France. An oscillation range of 0.1° was used during data collection. The crystal diffracted to a resolution of 2.1 Å. Data were processed and scaled using the software package XDS(1).

The SBV virion crystals were of space group C2. Rotation function plots and packing considerations indicated that 1/2 of a virus particle occupied a crystallographic asymmetric unit. One of the icosahedral twofold axes of symmetry of the capsid was superimposed with a crystallographic twofold axis. A one-dimensional search using an icosahedral locked self-rotation function was used to determine the rotation of the particle about the crystallographic twofold axis, calculated using the program GLRF(2). Reflections between resolutions of 6.0 and 4.5 Å were used for the calculations. The results showed that the particle was rotated by 127.51° about the twofold axis from the standard icosahedral orientation as described by Rossmann and Blow(3) when using the XYK polar angle convention. Because of the superposition of the icosahedral and crystallographic symmetry, the center of the particle had to be positioned on a crystallographic twofold axis. The PDB structure of SBPV converted to polyalanine with the P-domains of VP3 deleted was used for the molecular replacement. The appropriately oriented model was positioned onto the twofold axis and an initial low-resolution electron density map was calculated. The positions of the subunits were subjected to rigid-body refinement using the program suite Phenix(4). The new model was used to calculate phases to a resolution of 10 Å in the program CNS(5). The phases were refined by 25 cycles of averaging with the program AVE(6), using thirty-fold non-crystallographic symmetry. Phase extension was applied in order to obtain phases for high-resolution reflections. The addition of a small fraction of higher-resolution data (one index at a time) was followed by three cycles of averaging. This procedure was repeated until phases were obtained for all the reflections to a resolution of 2.1 Å. The model was rebuilt manually using the program Coot(7) alternating with coordinate refinement in the program CNS. Other calculations were done using the CCP4 program suite(8).

Cryo-EM data acquisition and image processing. The following samples were used for cryo-EM analyses: (1) freshly purified SBV in PBS; (2) SBV incubated in PBS buffer of pH 5.8 at 34°C for 20 min. A suspension of SBV (3.8 μl at concentration 2 mg/ml) was applied onto holey carbon coated grids (R2/1, mesh 300; Quantifoil Micro Tools) and vitrified by plunging into liquid ethane using an FEI Vitrobot™ Mark IV. Grids with the vitrified sample were transferred to an FEI Titan Krios electron microscope operated at 300 kV aligned for parallel illumination in nanoprobe mode. The sample in the column of the microscope was kept at -196°C. Images were recorded with a FEI Falcon II direct electron detection camera under low-dose conditions (17 $e^-/Å^2$) with underfocus values ranging from 1.0 to 2.7 μm at a nominal magnification of 75,000 x, resulting in a pixel size of 1.063 Å/px. Each image was recorded in movie mode with 0.41 seconds of total acquisition time and saved as seven movie frames. The frames from each exposure were aligned to compensate for drift and beam-induced motion using MotionCorr(9) followed by optical flow alignment using the program Xmipp(10).

Single particle reconstruction of SBV virion and expanded empty particles. Regions of the images containing the SBV particles were picked from the micrographs using the program e2boxer.py from the EMAN2(11) package and extracted from micrographs using the program RELION(12) (546 x 546 pixels boxsize). Contrast transfer function (CTF) parameters of each micrograph were automatically estimated using the program CTFFIND4(13). The images were processed using the package RELION(12). The structure of the IAPV virion (EMD-4114) determined by cryo-EM was used to initiate the reconstruction(14). The initial model was low-pass filtered to a resolution of 60 Å. The dataset was subjected to multiple rounds of 2D and 3D classifications, resulting in near-homogeneous sets of full and empty SBV particles. In the dataset of SBV particles exposed to low pH, two expansion intermediates of the empty particles were identified. Refinement according to "gold-standard" was performed using the RELION 3dautorefine procedure, with the starting model from the previous 3D classification reconstruction low-pass filtered to a resolution of 60 Å. The reconstructions were followed by another round of 3D classification, where the alignment step was omitted and the estimated orientations and particle center positions from the previous refinement step were used. The final reconstruction was performed using the RELION 3dautorefine. The resulting unfiltered electron density maps were masked by threshold masks, created using the RELION mask_create routine. To avoid over-masking, the masked maps were visually inspected to exclude the possibility of the clipping of electron densities belonging to the virus capsid. Additionally, the occurrence of over-masking was monitored by inspecting the shape of FSC curve. Furthermore, the shapes of the FSC curves of phase-randomized half-datasets with the applied mask were checked. The resulting resolutions of the reconstructions were estimated as the values at which the FSC curves fell below 0.143(15).

Cryo-EM structure determination and refinement. Model of SBV obtained from crystal structure (pdb:5LSF) was rigid body fitted into the B-factor-sharpened cryo-EM maps of SBV using Chimera(16) and subjected to manual rebuilding using the program Coot. Cryo-EM maps were re-oriented so that a subset of three perpendicular twofold icosahedral symmetry axes of the capsid was aligned with the Cartesian coordinate axes. The maps were cropped, normalized, and set to crystallographic P23 symmetry. This treatment of the maps resulted in five icosahedral asymmetric units in one "crystallographic" asymmetric unit of the P23 space group and enabled efficient refinement of the structures in reciprocal space. Reciprocal space refinement in program REFMAC5 was used utilizing the electron scattering structure factors library (atomsf_electron.lib)(17). Weight matrix value was optimized to achieve good agreements with experimental maps while preserving acceptable molecular geometries. For refinement of "Empty particle pH 5.8 expansion state II" the temperature factors of all atoms were set to a fixed value of 200 $Å^2$ because at this resolution the temperature factor refinement did not converge to meaningful values. Resulting models for full virions and empty particles were deposited to PDB database under separate codes (Table S1). Analyses of pentamer movements, specifically calculations of center of mass, were performed with Moleman2 from USF software package(18).

Cloning, expression and purification of His_6-SUMO-MiCP fusion protein. The nucleotide sequence of the SBV MiCP (residues 711–755 of the polyprotein) was cloned into the expression plasmid pET22T under the control of the T7 promoter. The vector provided the N-terminal His_6-SUMO tag (Smt3 from *S. Cerevisiae*; 12 kDa). LB media supplemented with ampicillin (100 μg/ml) was inoculated with *E. coli* BL21(DE3) containing the above-mentioned plasmid. The culture was cultivated at 37°C until an optical density at 600 nm reached value of 0.4–0.6. Protein expression was induced by addition of isopropyl β-D-1-thiogalactopyranoside (IPTG) to a final concentration of 0.3 mM, and the culture was cultivated at 37°C for 5 h with 250 RPM orbital shaking. Cells from 500 ml of media were collected by centrifugation and re-suspended in 3 ml of BugBuster® reagent (Merck) supplemented with 1 mg/ml lysozyme, 5 μg/ml DNAse I, 10 μg/ml RNAse, and 100 μg/ml Protease inhibitor cocktail (Sigma-Aldrich). The resulting mixture was incubated for 60 min at room temperature. The lysate was clarified by centrifugation at 20,000 g at 4°C for 20 min. The resulting supernatant was supplemented with imidazole to a final concentration of 20 mM, loaded on a HisTrap™ HP column (GE Healthcare), and the protein of interest was eluted with a gradient of imidazole (20–500 mM) in PBS. All elution fractions were analyzed using SDS–PAGE and those containing the highest amounts of His_6-SUMO-MiCP protein were concentrated using a centrifugal concentrator (MW cutoff 10,000 Da). The concentrated material was digested with Ulp1 protease in a reaction mixture containing 30 mM DTT and 1 mM PMSF for 16 h at room temperature. The resulting mixture was purified using a HisTrap™ HP column. All fractions were analyzed on 10–20% SDS gradient gel (Novagene) and the flow-through fractions containing MiCP were concentrated in a centrifugal concentrator (MW cut-off 5,000 Da). The identity of the protein was verified by mass spectrometry analysis of a liquid sample with a final concentration of 4.0 mg/ml (determined by A_{280}). Purified MiCP was used for the fluorescence assay described below.

Fluorescence assay of liposome integrity. Liposomes were prepared as described previously(19), briefly: 1 ml of phospholipid mixture (Avanti lipids) corresponding to the composition of the late endosome membrane(20) (45% phosphatidyl choline, 18% phosphatidyl ethanolamine, 14% bis(monoacylglycerol)phosphate, 9% phosphatidyl inositol, 9% cholesterol, 5% phosphatidyl serine) was diluted in 5 ml of chloroform. The mixture was pipetted into a 1 L evaporation flask connected to a vacuum rotary evaporator (Heidolph), and the solvent was evaporated at 50 RPM, at 37°C for 1 h, at a pressure of 200 mbar. The resulting lipid film was re-hydrated in 5 ml of reconstitution buffer (50 μM carboxyfluorescein, 10 mM HEPES pH 7.0) by rotating on an evaporator for 60 min, at room temperature and atmospheric pressure. Reconstituted opalescent solution was sonicated (Sonica, SOLTEC) in an ice bath for 10 min and subsequently extruded through 400 nm filters in 500 μl batches using an Avestin extruder (Avestin). Extruded liposomes were pelleted at 20,000 g at 4°C for 15 min and used for subsequent experiments.

The increase in the fluorescence signal upon release of carboxyfluorescein from liposomes was measured using a FluostarOMEGA plate reader (BMG labtech) at an excitation wavelength of 485 nm and emission wavelength of 520 nm. Two reaction conditions were tested: native pH in HEPES buffer (155 mM NaCl, 10 mM Hepes, pH 7.4), and low pH in MES buffer

(155 mM NaCl, 10 mM MES, pH 5.5). For the 100 μl reaction, 10 μl of liposome solution was diluted with the respective reaction buffer and pipetted into black-walled 96-well plates for fluorescence measurements. After 50 s incubation, 10 μl of solution containing either MiCP at the final concentration 2 μM or SBV virions at the final concentration 2 nM (which corresponds to 120 nM concentration of MiCP) were injected using the automatic injector system of the FluostarOMEGA plate reader. After another 100 s of incubation, 10 μl of Triton X-100 at the final concentration of 1% were injected. Changes in the fluorescence signal in response to the addition of MiCP, SBV or Triton X-100 were recorded as fluorescence values in arbitrary units. The negative control of the pH effect was performed by addition of the reaction buffer instead of MiCP or SBV. For comparison and plotting, the values were normalized using the equation: $X_{norm} = (X–X_{min})/(X_{max}–X_{min})$. The plotted values are an average of three repetitions.

Mass spectrometry analyses. The virus protein fraction resulting from the TRI Reagent® separation procedure was re-suspended in Laemli buffer and subjected to SDS–PAGE on a tricine gradient gel. The protein bands corresponding to capsid proteins of SBV were excised from the gel and used for mass spectrometry analysis. In parallel, material from whole SBV virions treated with SDS loading buffer was analyzed. After destaining and washing, the proteins were incubated with trypsin (sequencing grade; Promega). MALDI-MS and MS/MS analyses were performed on an Ultraflextreme mass spectrometer (Bruker Daltonics, Bremen, Germany). Alternative digestions were performed with chymotrypsin and pepsin. The software FlexAnalysis 3.4 and MS BioTools 3.2 (Bruker Daltonics) were used for data processing. Exported MS/MS spectra were searched using in-house Mascot software (Matrixscience, London, UK; version 2.4.1) against the NCBI database (no taxonomy restriction) and a local database supplied with the expected sequence. The mass tolerances of peptides and MS/MS fragments for MS/MS ion searches were 50 ppm and 0.5 Da, respectively. Oxidation of methionine and propionylamidation of cysteine as optional modifications and one enzyme mis-cleavage were set for all searches. Peptides with a statistically significant peptide score ($p < 0.05$) were considered.

Sequencing of SBV P1 region. Total virus RNA was isolated from purified virions(21), subjected to reverse transcription and the resulting cDNA was sequenced using specific primers designed to cover the P1 region of the SBV polyprotein. The resulting sequences were assembled using the software Geneious version R10(22).

Phylogenetic analyses. Multiple sequence alignment was performed using MAFFT, specifically the E-INS-i strategy (23) and trimmed using the program Trimal(24). Maximum likelihood phylogenetic tree was constructed with the program W-IQ-Tree (25). The rendering was carried out using Geneious R10 software (22). Structure-based pairwise alignments of the VP3 subunits of various viruses were prepared using the program VMD(26). The similarity score provided by VMD was used as an evolutionary distance to construct a nexus-format matrix file, which was converted into the phylogenetic tree and visualized with the program FigTree v1.4.3.

Data deposition

Cryo-EM maps of the SBV virions from the different conditions were deposited in electron microscopy data (EMDB) bank under the following accession numbers: 3863 (native virion pH 7.4), 3881 (empty particle pH 7.4), 3865 (virion pH 5.8), 3866 (empty particle pH 5.8, expansion state I), and 3867 (empty particle pH 5.8, expansion state II); and the corresponding coordinates were deposited in protein data bank (PDB) under the following accession numbers: 5OYP (native virion pH 7.4), 6EIW (empty particle pH 7.4), 6EGV (virion pH 5.8), 6EGX (empty particle pH 5.8, expansion state I), and 6EH1 (empty particle pH 5.8, expansion state II). The crystal structure of the SBV virion was deposited under PDB accession number 5LSF. The consensus nucleotide sequence of the SBV capsid proteins was deposited in GenBank under accession number KY617033.

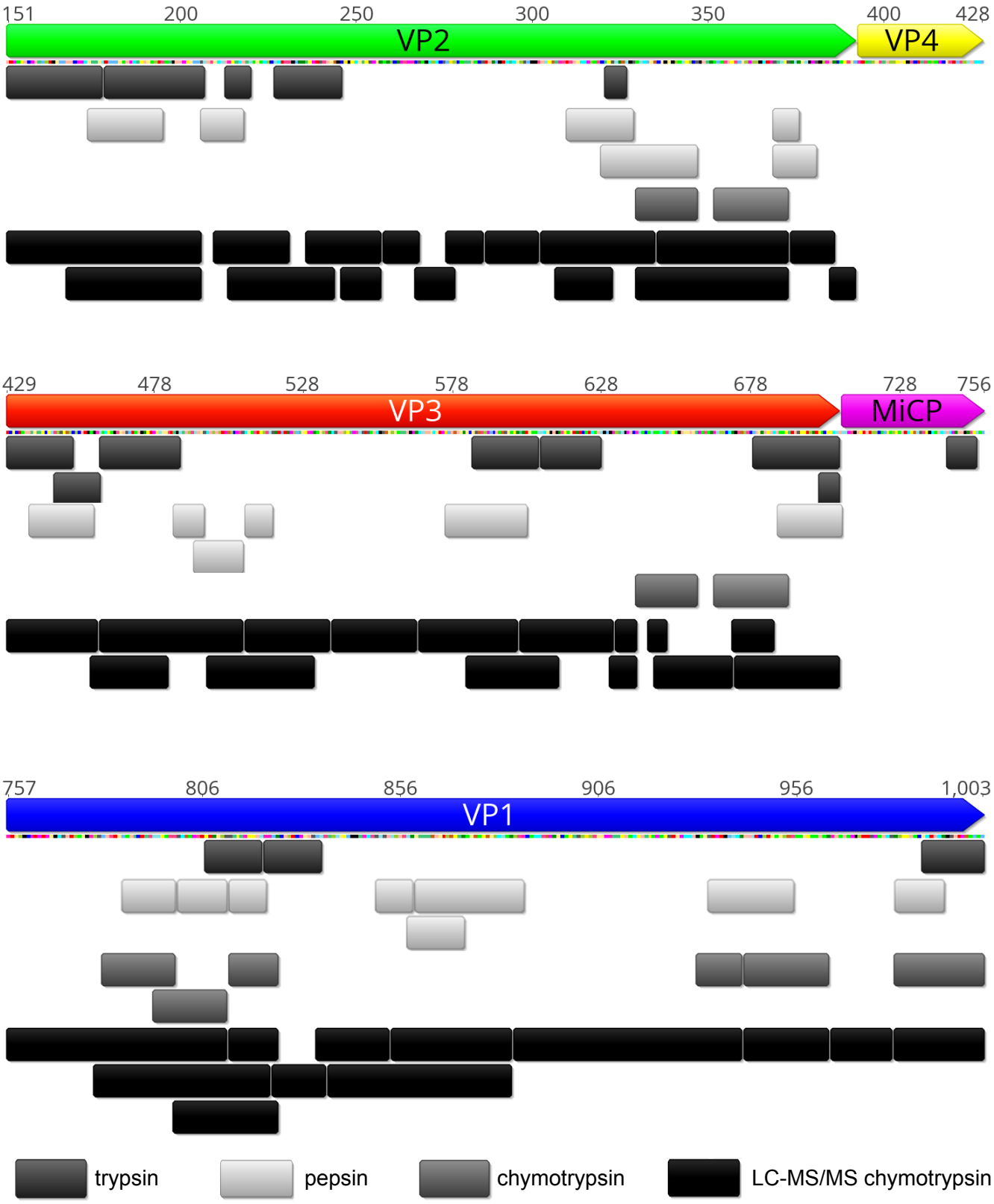

Fig. S1. Mass spectrometry analysis of SBV capsid proteins. Parts of P1 polyprotein of SBV are indicated in blue for VP1, green for VP2, red for VP3, yellow for VP4, and magenta for MiCP. Peptide fragments identified by mass spectrometry analyses are indicated below the polypeptide as boxes with various shades of grey. Four types of analyses were done: pepsin digest, trypsin digest, chymotrypsin digests each followed by MS, and chymotrypsin digest combined with LC-MS/MS analysis.

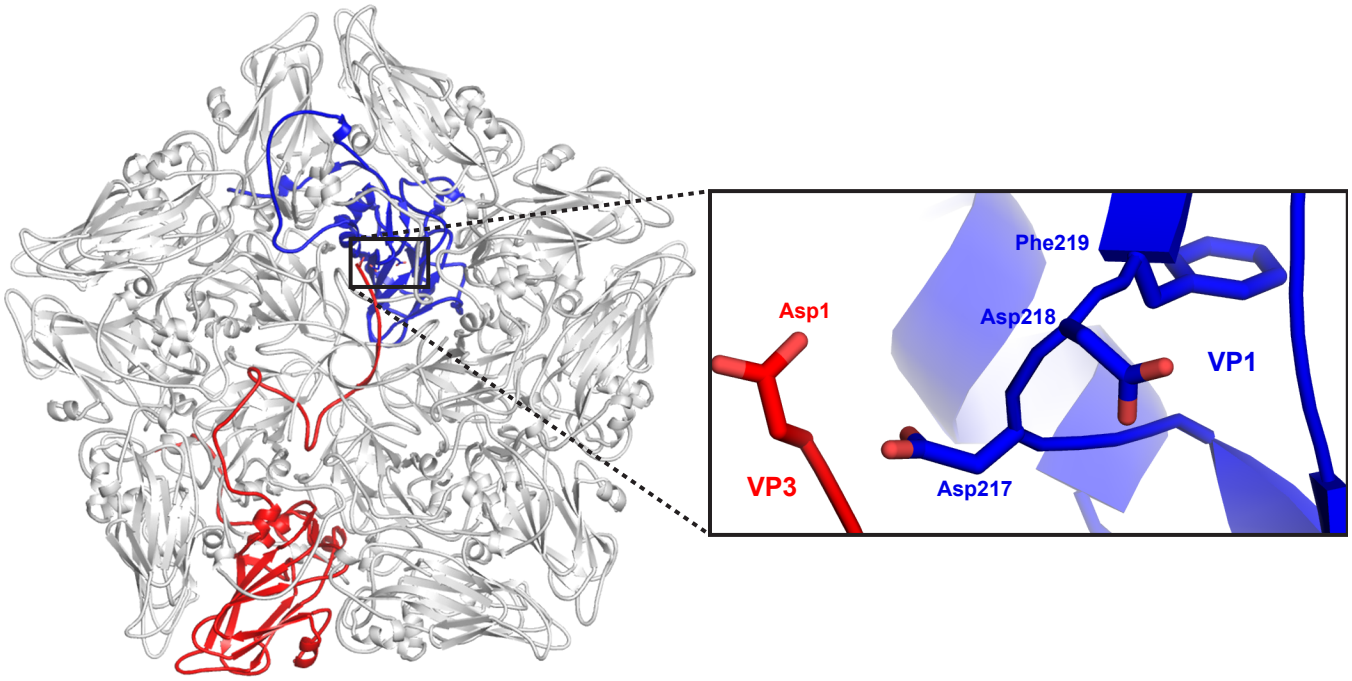

Fig. S2. Conserved motif Asp–Asp–Phe (DDF) of SBV VP1 may catalyze cleavage of VP0 into VP3 and VP4 fragments. Pentamer of SBV protomers with one selected VP3 subunit highlighted in red and VP1 subunit from another ASU in blue. The DDF residues of the selected VP1 subunit are close to the N-terminus of the selected VP3 subunit. Detail of interaction of DDF motif and N-terminal amino acid of VP3; side chains are represented as sticks.

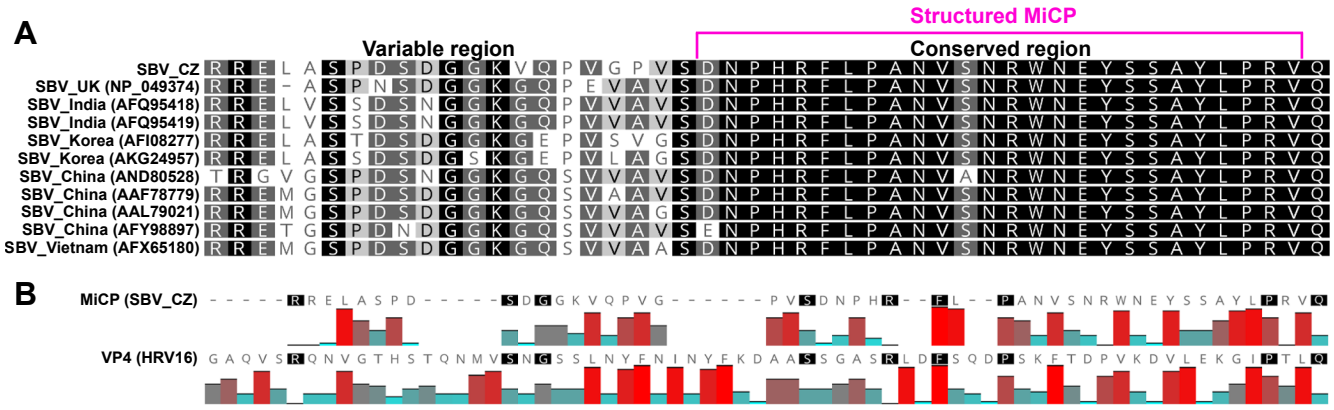

Fig. S3. Amino acid sequence analysis of MiCP. Protein sequence comparison of MiCPs from various SBV isolates (A). MiCP can be divided into variable N-terminal and conserved C-terminal parts. The conserved part is resolved in the virion structures. Sequences were aligned using the software Geneious (R10). The amino acid sequence of VP4 of human rhinovirus 16 was aligned onto that of MiCP based on similar hydrophobicity profiles (B). The hydrophobicity plots are depicted as histograms below the sequences. Hydrophobic residues are highlighted in red and hydrophilic in blue.

Fig. S4. Alignment of polyprotein sequences of selected iflaviruses. Sequences were aligned using MAFFT tools, E-ENS-i method, and trimmed with Trimal tool (24). Sequences were obtained from NCBI database, given ID numbers refer to Genome depository with exception of SBV_CZ, which was deposited to GenBank. CRPV-gp2 – Cricket paralysis virus (ID: 5001) (included as out-group); PNIV – Perina nuda virus (ID: 4901); EOPV – Ectropis obliqua picorna-like virus (ID: 5110); SBPV – Slow bee paralysis virus (ID: 3992); DWV – Deformed wing virus (ID: 5055); VDV – Varroa destructor virus (ID: 5239); FEV – Formica exsecta virus 2 (ID: 23898); BMV – Bombyx mori iflavirus (ID: 39939); SBV_CZ – Sacbrood virus, CZ Petrusov isolate (GenBank: KY617033); SBV_UK – Sacbrood virus 'Rothamsted' (ID: 4872); LIV-1 – Ligus linoelaris virus 1; LJV - La Jolla virus (ID: 38343); HHV – Halyomorpha halys virus (ID: 23003); IFV – Infectious flacherie virus 1 (ID: 4972); OPV – Opsiphanes invirae iflavirus 1 (ID:40416).

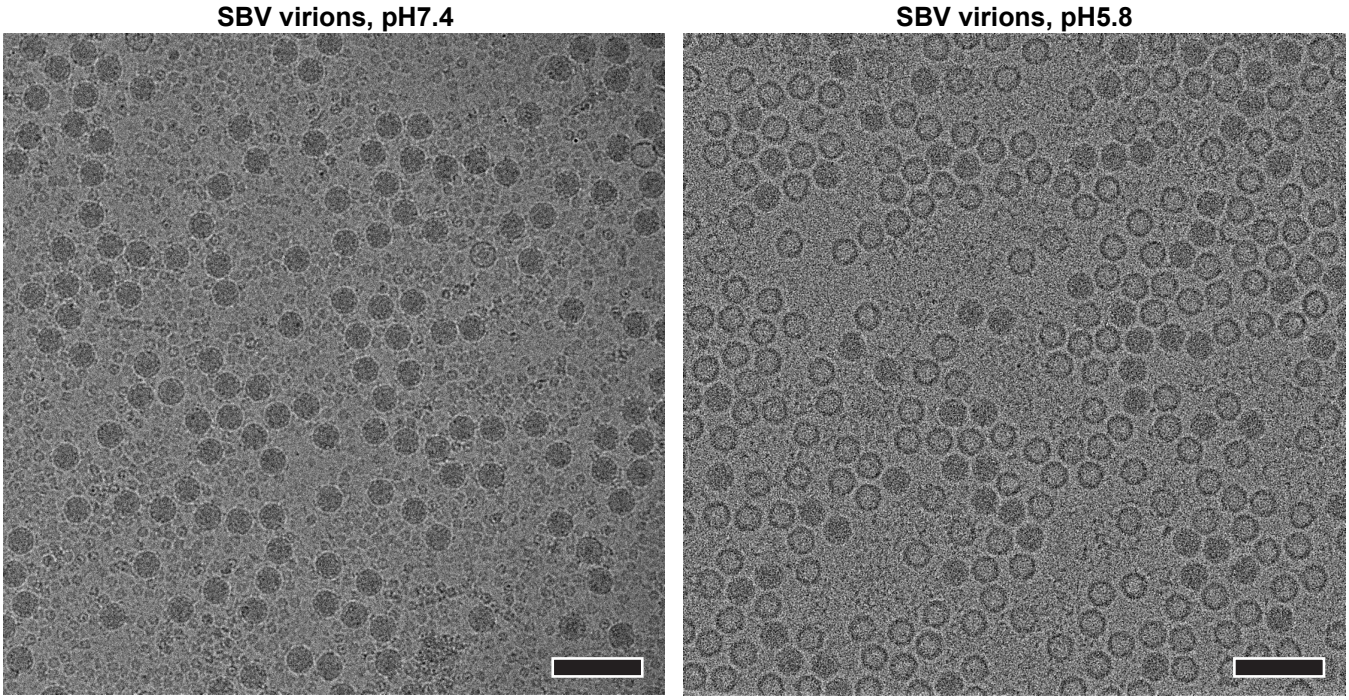

Fig. S5. Low pH induces genome release of SBV. Representative cryo-electron micrographs of SBV particles in buffers of pH 7.4 (A) and 5.8 (B). Small particles in the background correspond to contamination with honeybee protein hexamerin.

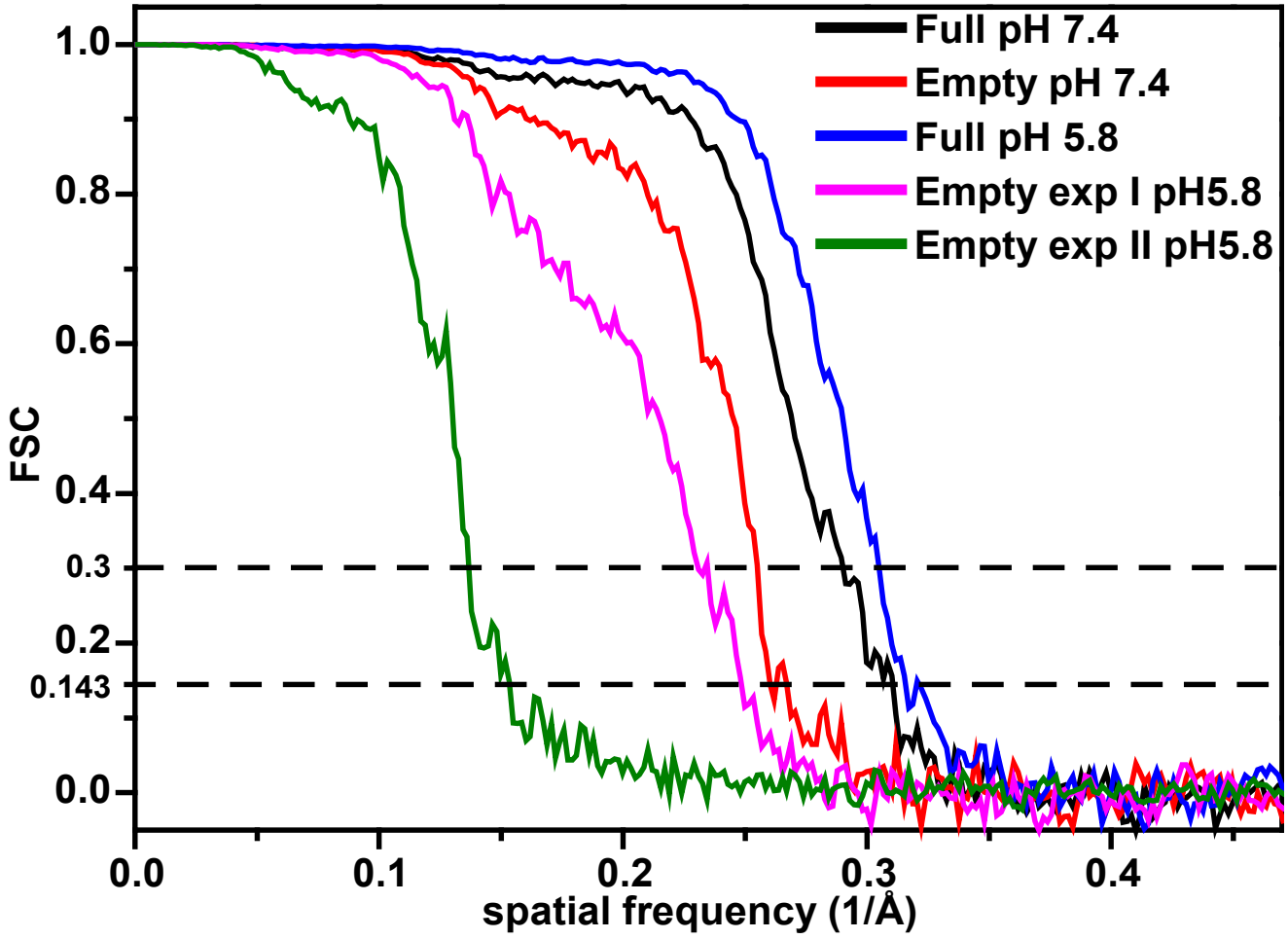

Fig. S6. FSC curves of cryo-EM reconstructions of SBV virions and empty particles under different conditions. The FSC of the native SBV virion at pH 7.4 is shown in black, empty particle at pH 7.4 in red, SBV virion at pH 5.8 in blue, less expanded empty particle at pH 5.8 in magenta, and more expanded empty particle at pH 5.8 in green.

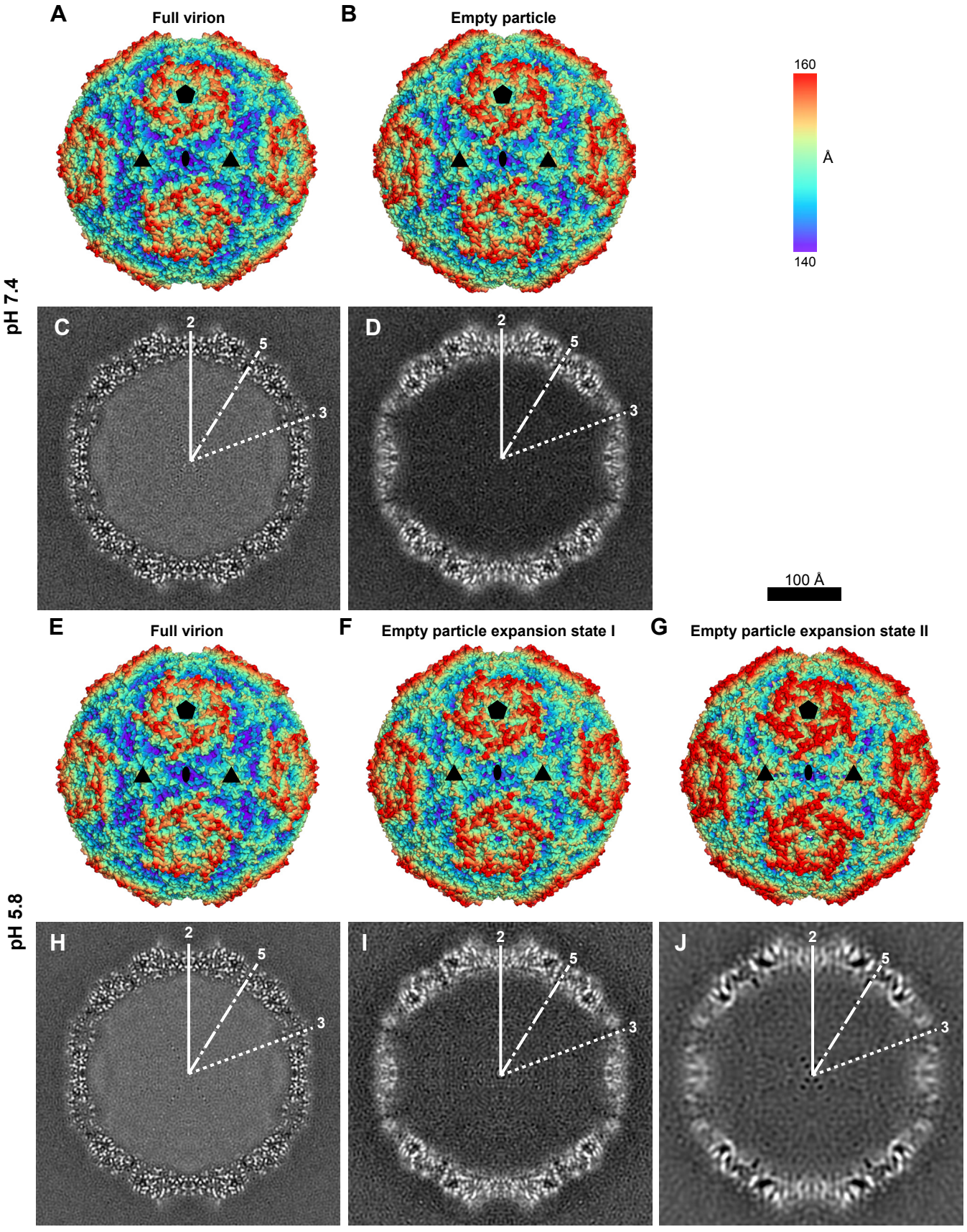

Fig. S7. Effect of low pH on SBV virions. Cryo-EM reconstructions of SBV particles under native conditions (pH 7.4): virion (A) and empty particle (B). SBV particles at pH 5.8: genome containing virions (E), empty expansion intermediate I (F), and empty expansion intermediate II (G). The molecular surfaces of the respective particles are rainbow-colored according to their distance from the particle center. The locations of the selected symmetry axes are denoted by pentagons for fivefold, triangles for threefold, and ellipses for twofold. Scale bar 100 Å. Central slices of electron density maps are shown in the bottom row (C, D, H, I, J). White areas indicate areas with high electron density values. The positions of selected icosahedral symmetry axes are labeled.

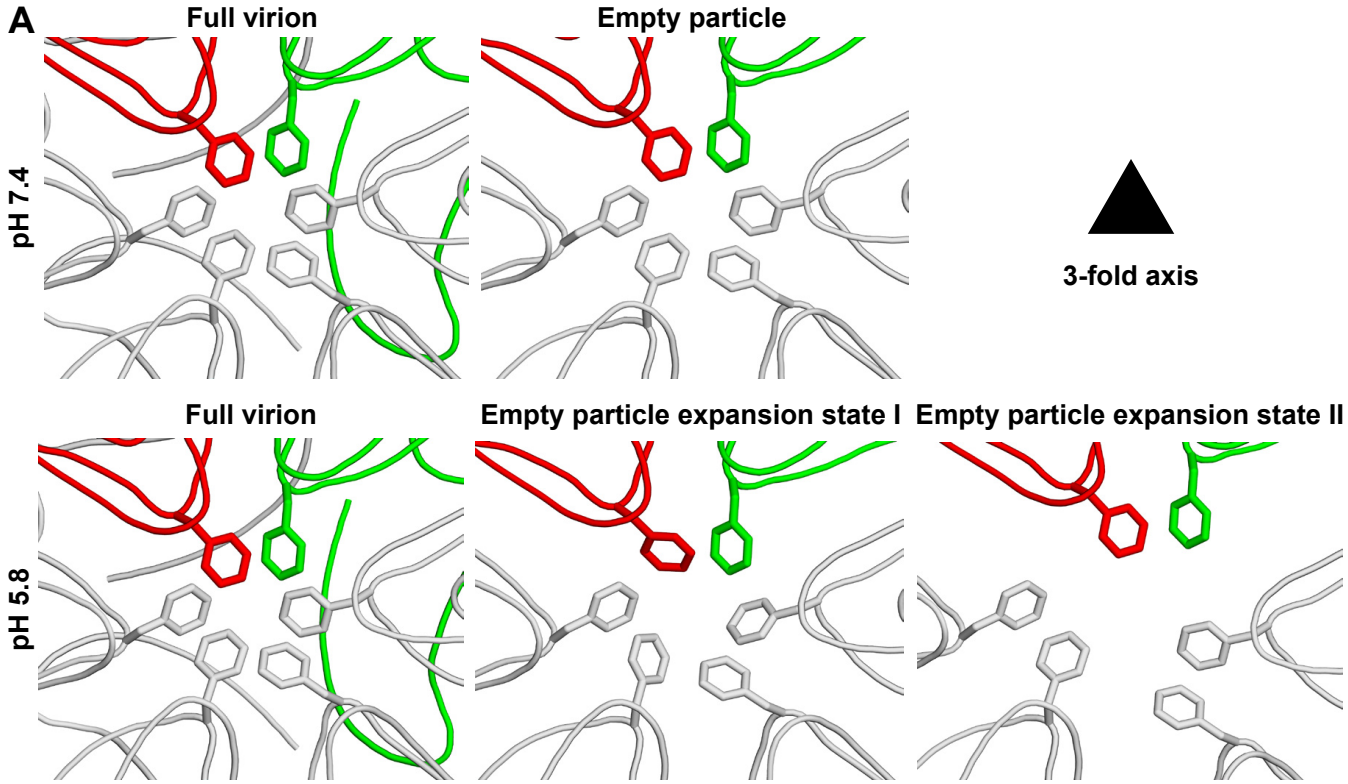

Fig. S8. Comparison of capsid structures close to icosahedral axes of symmetry of SBV virions and empty particles. *(Continued on next page....)*

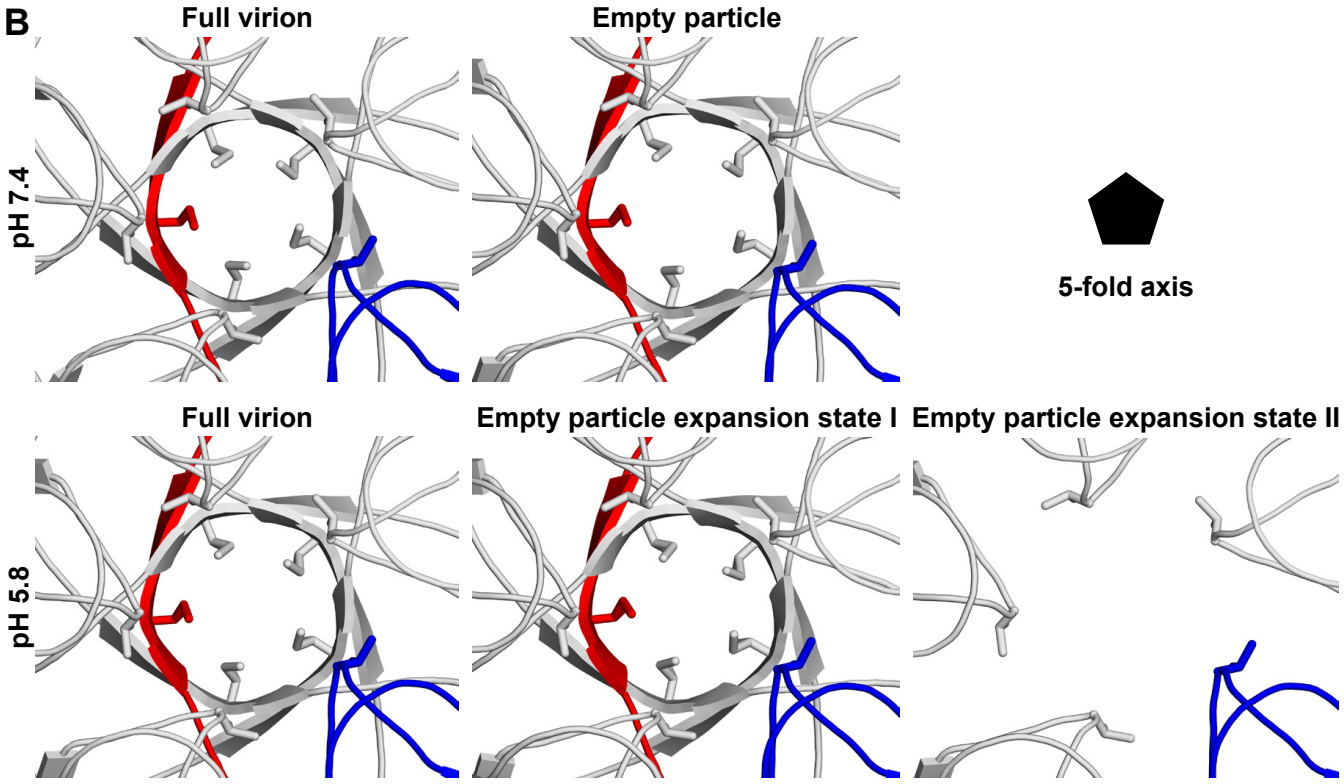

Fig. S8. Comparison of capsid structures close to icosahedral axes of symmetry of SBV virions and empty particles. *(Continued on next page....)*

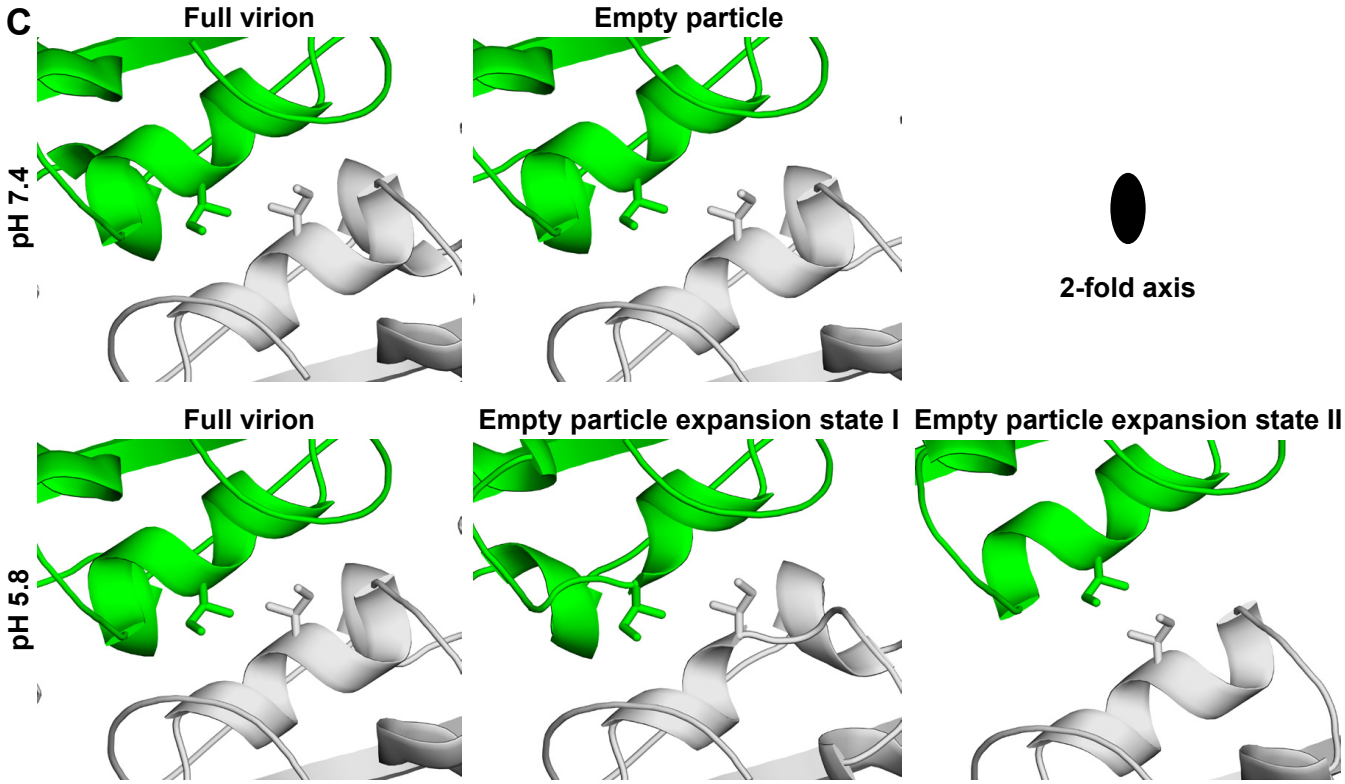

Fig. S8. Comparison of capsid structures close to icosahedral axes of symmetry of SBV virions and empty particles. The capsid protein loops in the vicinity of the symmetry axes are shown in cartoon representation. VP1, VP2, and VP3 from one selected icosahedral asymmetric unit are shown in blue, green, and red, respectively. Side chains of residues closest to the threefold axis are shown as sticks. Details of threefold (A), fivefold (B), and twofold (C) symmetry axes.

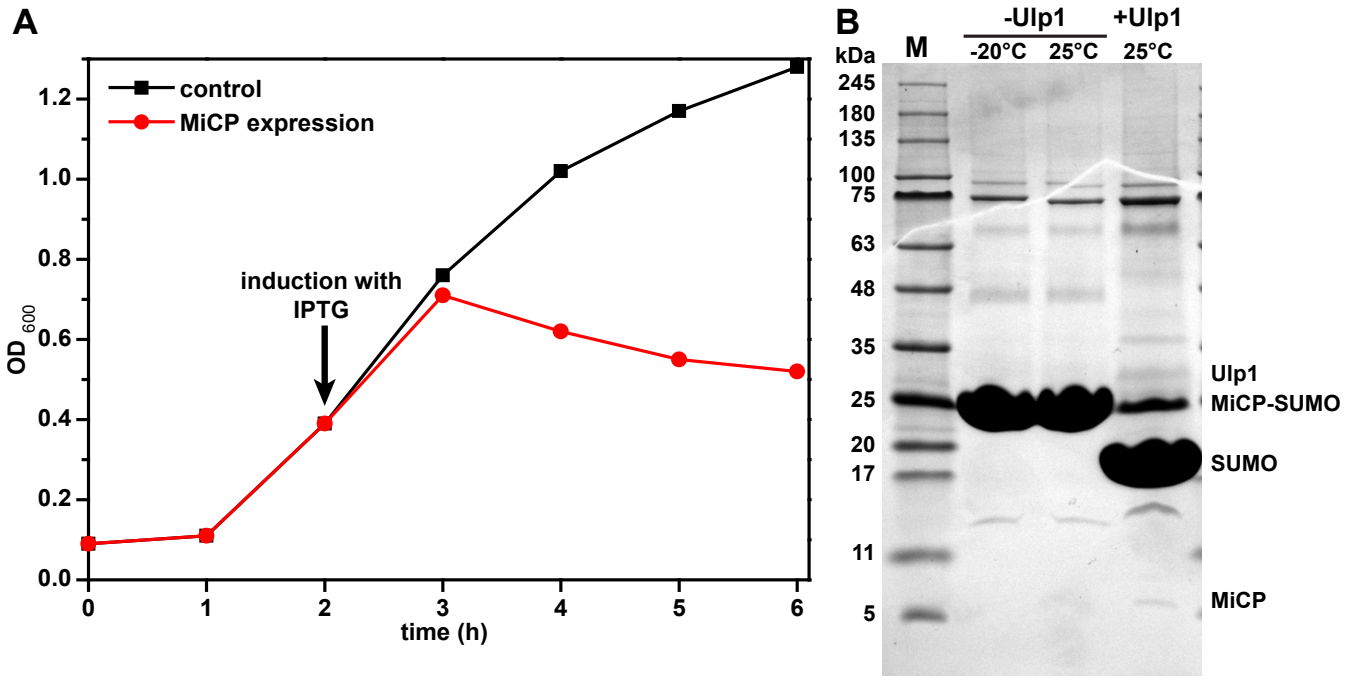

Fig. S9. Effect of MiCP expression on growth of bacterial cells. (A) Expression of MiCP with N-terminal His_6-SUMO tag was induced by addition of IPTG to culture media at 2 hours (red line). Control cells contained empty expression vector (black line). (B) MiCP remained soluble after His_6-SUMO tag cleavage using Ulp1 protease.

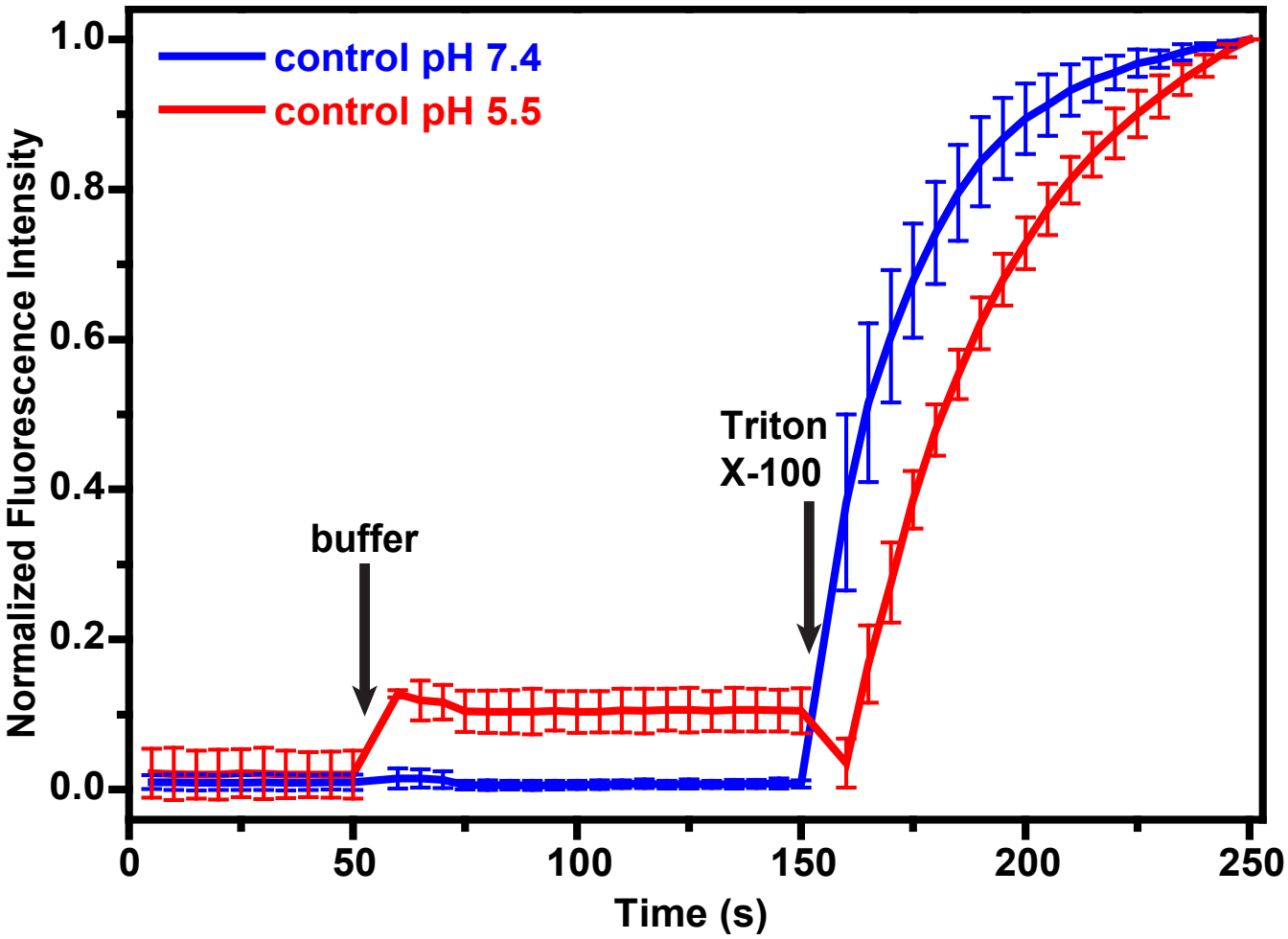

Fig. S10. Negative control for disruption of liposomes at pH 5.5. Liposomes containing carboxyfluorescein were transferred to a solution with pH 7.4 (black line) or pH 5.5 (red line). After 50 s incubation, 10 μl of the same buffer was added to liposomes and incubated for 150 s when the liposomes were dissolved with 1% Triton X-100. The measured fluorescence values were normalized and plotted as an average of three independent experiments with standard deviations.

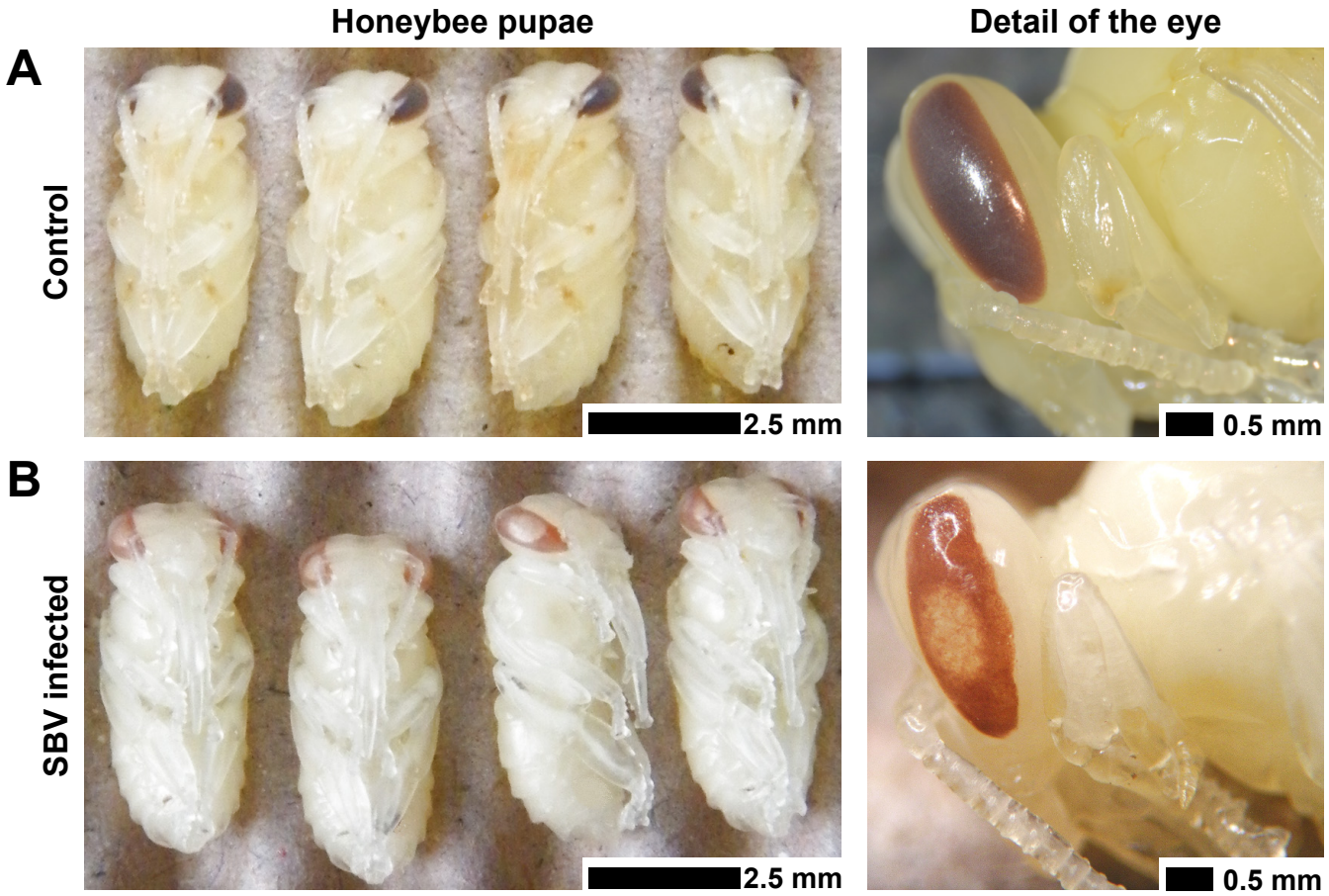

Fig. S11. Phenotype of high-titer SBV infection in pupae. White-eyed pupae were infected with SBV inoculum. Infected and control pupae were inspected five days after infection. The compound eyes of control pupae are fully and regularly pigmented (A). In contrast the eyes of infected pupae contain white areas at their centers (B).

Table S1. Data and structure quality indicators of SBV virions and empty particles.

Crystal structure		Cryo-EM structure					
		3863	3881	3865	3866	3867	EMDB
PDB	5LSF	5OYP	6EIW	6EGV	6EGX	6EH1	PDB
Space group	C 121	75 000x	75 000x	75 000x	75 000x	75 000x	Magnification
a, b, c (Å)	487.8, 360.9, 337.9	1.0 - 2.7	1.0 - 2.7	1.0 - 2.7	1.0 - 2.7	1.0 - 2.7	Defocus range (μm)
α, β, γ (°)	90, 133, 90	17	17	17	17	17	Electron exposure (e^-/Å^2)
Resolution range# (Å)	47.0 - 2.1 (2.14 - 2.10)	3.22	3.87	3.18	4.06	7.25	Map resolution (Å)
R_{merge}	0.135 (0.639)	0.143	0.143	0.143	0.143	0.143	FSC treshold
<I>/ <σI>	6.6 (1.0)	icosahedral	icosahedral	icosahedral	icosahedral	icosahedral	Symmetry imposed
Completeness# (%)	64.0 (21.5)	1.063	1.063	1.063	1.063	1.063	Pixel size (Å)
Redundancy#	3.1 (1.4)	31 804	31 804	51 117	51 117	51 117	Initial particles (no.)
No. of unique reflections#	1 572 812 (27 056)	10 303	16 106	13 148	2341	5330	Final particles (no.)
R factor+	0.192	0.341	0.371	0.341	0.405	0.488	R factor+
No. of atoms§	6 230	6 233	5 806	6 233	5 822	5 157	No. of atoms§
RMSD bond lengths (Å)	0.0068	0.004	0.004	0.004	0.004	0.004	RMSD bond lengths (Å)
RMSD bond angles (°)	1.45	0.95	0.94	0.93	0.92	0.92	RMSD bond angles (°)
Ramachandran favored (%)*	95.73	93.4	95.26	95.73	94.44	94.47	Ramachandran favored (%)*
Ramachandran allowed (%)*	4.01	6.34	4.46	4.27	5.56	5.53	Ramachandran allowed (%)*
Ramachandran outliers (%)*	0.26	0.26	0.28	0	0	0	Ramachandran outliers (%)*
Poor rotamers (%)*	4.05	1.59	0.16	0.43	0.31	0.35	Poor rotamers (%)*
Clashscore (percentile)*	6.11 (97)	0.98 (100)	0.52 (100)	0.65 (100)	0.61 (100)	1.18 (100)	Clashscore (percentile)*
MolProbity score (percentile)*	2.09 (74)	1.37 (100)	1.01 (100)	1.01 (100)	1.08 (100)	1.21 (100)	MolProbity score (percentile)*
Cβ deviations (%)*	0	0	0	0	0	0	Cβ deviations (%)*

The statistics for the highest resolution shell are shown in parentheses; $R_{merge} = \Sigma_h \Sigma_j \mid |I_{hj}| - |<I_h>| \mid / \Sigma\Sigma \mid I_{hj} \mid$.

+ All reflections were used in the refinement. The R_{free}, if it were calculated, would be very similar to R_{work} because of the 30-fold non-crystallographic symmetry present in the crystal. Therefore, R_{free} would not provide an unbiased measure of model quality in this case(27).

§ statistics are given for one icosahedral asymmetric unit.

* values according to Molprobity(28).

Please note that right side of the table contains values for cryo-EM data: accelerating voltage - 300 kV; initial model – IAPV (EMD-4114).

Table S2. Comparison of protomer structures of SBV particles under different conditions.

	SBV crystal structure	Virion pH 7.4	Empty particle pH 7.4	Virion pH 5.8	Empty particle pH 5.8 exp. state I.
Virion pH 7.4	0.439 (100)	-	-	-	-
Empty particle pH 7.4	0.447 (93)	0.357 (93)	-	-	-
Virion pH 5.8	0.321 (100)	0.268 (100)	0.275 (93)	-	-
Empty particle pH 5.8 exp. state I.	0.610 (93)	0.471 (93)	0.421 (93)	0.472 (93)	-
Empty particle pH 5.8 exp. state II.	0.464 (82)	0.401 (82)	0.313 (82)	0.336 (82)	0.505 (82)

Root-mean-square deviations (RMSD, Å) of superimposed Cα atoms of protomers of respective SBV structures. The number in parenthesis indicates the percentage of available amino acid residues used for the calculations. The icosahedral asymmetric units consisting of subunits VP1, VP2 and VP3 were used as rigid bodies in the calculations. The cutoff for the inclusion of residues for the RMSD calculation was 3.8 Å.

References

1. Kabsch W (2010) Xds. *Acta Crystallographica Section D: Biological Crystallography* 66(2):125–132.
2. Tong L, Rossmann MG (1997) Rotation function calculations with GLRF program. *Methods in Enzymology* 276(1964):594–611.
3. Rossmann MG, Blow DM (1962) The detection of sub-units within the crystallographic asymmetric unit. *Acta Crystallographica* 15(1):24–31.
4. Adams PD, et al. (2010) PHENIX: A comprehensive Python-based system for macromolecular structure solution. *Acta Crystallographica Section D: Biological Crystallography* 66(2):213–221.
5. Brunger AT (2007) Version 1.2 of the crystallography and nmr system. *Nature protocols* 2(11):2728.
6. Kleywegt GJ, Read RJ (1997) Not your average density. *Structure* 5(12):1557–69.
7. Emsley P, Lohkamp B, Scott WG, Cowtan K (2010) Features and development of Coot. *Acta Crystallographica Section D: Biological Crystallography* 66(4):486–501.
8. Winn MD, et al. (2011) Overview of the CCP4 suite and current developments. *Acta crystallographica. Section D, Biological crystallography* 67(Pt 4):235–42.
9. Li X, et al. (2013) Electron counting and beam-induced motion correction enable near-atomic-resolution single-particle cryo-em. *Nature methods* 10(6):584.
10. Sorzano C, et al. (2004) Xmipp: a new generation of an open-source image processing package for electron microscopy. *Journal of structural biology* 148(2):194–204.
11. Tang G, et al. (2007) EMAN2: An extensible image processing suite for electron microscopy. *Journal of Structural Biology* 157(1):38–46.
12. Scheres SHW (2012) RELION: Implementation of a Bayesian approach to cryo-EM structure determination. *Journal of Structural Biology* 180(3):519–530.
13. Rohou A, Grigorieff N (2015) Ctffind4: Fast and accurate defocus estimation from electron micrographs. *Journal of structural biology* 192(2):216–221.
14. Mullapudi E, Füzik T, Přidal A, Plevka P (2017) Cryo-electron microscopy study of the genome release of the dicistrovirus israeli acute bee paralysis virus. *Journal of virology* 91(4):e02060–16.
15. Scheres SHW, Chen S (2012) Prevention of overfitting in cryo-EM structure determination. *Nature Methods* 9(9):853–854.
16. Pettersen EF, et al. (2004) Ucsf chimera—a visualization system for exploratory research and analysis. *Journal of computational chemistry* 25(13):1605–1612.
17. Murshudov GN, Vagin AA, Dodson EJ (1997) Refinement of Macromolecular Structures by the Maximum-Likelihood Method. *Acta Crystallographica Section D* 53(3):240–255.
18. Kleywegt GJ, Jones TA (1997) [11] model building and refinement practice in *Methods in enzymology*. (Elsevier) Vol. 277, pp. 208–230.
19. Weissig V (2010) *Liposomes: Methods and protocols*. (Humana Press) Vol. 606.
20. van Meer G, Voelker DR, Feigenson GW (2008) Membrane lipids: where they are and how they behave. *Nature Reviews Molecular Cell Biology* 9(2):112–124.
21. Chomczynski P, Sacchi N (2006) The single-step method of rna isolation by acid guanidinium thiocyanate–phenol–chloroform extraction: twenty-something years on. *Nature protocols* 1(2):581.
22. Kearse M, et al. (2012) Geneious basic: an integrated and extendable desktop software platform for the organization and analysis of sequence data. *Bioinformatics* 28(12):1647–1649.
23. Katoh K, Rozewicki J, Yamada KD (2017) Mafft online service: multiple sequence alignment, interactive sequence choice and visualization. *Briefings in bioinformatics*.
24. Capella-Gutiérrez S, Silla-Martínez JM, Gabaldón T (2009) trimal: a tool for automated alignment trimming in large-scale phylogenetic analyses. *Bioinformatics* 25(15):1972–1973.
25. Trifinopoulos J, Nguyen LT, von Haeseler A, Minh BQ (2016) W-iq-tree: a fast online phylogenetic tool for maximum likelihood analysis. *Nucleic acids research* 44(W1):W232–W235.
26. Humphrey W, Dalke A, Schulten K (1996) VMD: Visual molecular dynamics. *Journal of Molecular Graphics* 14(1):33–38.
27. Kleywegt GJ, Brünger AT (1996) Checking your imagination: Applications of the free R value. *Structure* 4(8):897–904.
28. Hintze BJ, Lewis SM, Richardson JS, Richardson DC (2016) Molprobity's ultimate rotamer-library distributions for model validation. *Proteins: Structure, Function, and Bioinformatics* 84(9):1177–1189.